Interaction of carbon dioxide with Ni(110): A combined experimental and theoretical study

X. Ding
CNR-INFM DEMOCRITOS National Simulation Center, Theory@Elettra group, Area Science Park, Basovizza S.S. 14 Km 163.5, I-34012 Trieste, Italy

L. De Rogatis
Dipartimento di Scienze Chimiche e Centro di Eccellenza per i Materiali Nanostrutturati, Università di Trieste, via L. Giorgieri 1, I-34127 Trieste, Italy
and CNR-INFM Laboratorio Nazionale TASC, Area Science Park, Basovizza S.S. 14 Km 163.5, I-34012 Trieste, Italy

E. Vesselli, A. Baraldi, G. Comelli, and R. Rosei
Dipartimento di Fisica e Centro di Eccellenza per i Materiali Nanostrutturati, Università di Trieste, Via A. Valerio 2, I-34127 Trieste, Italy
and CNR-INFM Laboratorio Nazionale TASC, Area Science Park, Basovizza S.S. 14 Km 163.5, I-34012 Trieste, Italy

L. Savio and L. Vattuone
Dipartimento di Fisica, Università di Genova and CNISM, Unità di Genova, Via Dodecaneso 33, I-16146 Genova, Italy

M. Rocca
Dipartimento di Fisica, Università di Genova and IMEM-CNR, Sezione di Genova, Via Dodecaneso 33, I-16146 Genova, Italy

P. Fornasiero
Dipartimento di Scienze Chimiche e Centro di Eccellenza per i Materiali Nanostrutturati, Università di Trieste, via L. Giorgieri 1, I-34127 Trieste, Italy
and Italian Interuniversity Consortium on Materials Science and Technology (INSTM)

F. Ancilotto
Dipartimento di Fisica, Università di Padova, Via Marzolo 8, I-35131 Padova, Italy
and CNR-INFM DEMOCRITOS National Simulation Center, Trieste, Italy

A. Baldereschi
Dipartimento di Fisica Teorica, Università di Trieste, Strada Costiera 11, I-34014 Trieste, Italy;
CNR-INFM DEMOCRITOS National Simulation Center, Trieste, Italy;
and Institute of Theoretical Physics, École Polytechnique Fédérale de Lausanne (EPFL), CH-1015 Lausanne, Switzerland

M. Peressi
Dipartimento di Fisica Teorica, Università di Trieste, Strada Costiera 11, I-34014 Trieste, Italy
and CNR-INFM DEMOCRITOS National Simulation Center, Trieste, Italy
(Received 16 July 2007; revised manuscript received 17 September 2007; published 16 November 2007)

We present a combined experimental and theoretical study of the CO_2 interaction with the Ni(110) surface. Photoelectron spectroscopy, temperature-programmed desorption, and high-resolution electron energy loss spectroscopy measurements are performed at different coverages and for increasing surface temperature after adsorption at 90 K with the aim to study the competing processes of CO_2 dissociation and desorption. Simulations are performed within the framework of density functional theory using *ab initio* pseudopotentials, focusing on selected chemisorption geometries, determining the energetics and the structural and vibrational properties. Both experimental and theoretical vibrational frequencies yield consistent indications about two inequivalent adsorption sites that can be simultaneously populated at low temperature: short-bridge site with the molecular plane perpendicular to the surface and hollow site with the molecular plane inclined with respect to the surface. In both sites, the molecule has pure carbon or mixed oxygen-carbon coordination with the metal and is negatively charged and bent. Predicted energy barriers for adsorption and diffusion on the surface suggest a preferential adsorption path through the short-bridge site to the hollow site, which is compatible with the experimental findings. Theoretical results qualitatively support literature data concerning the increase of the work function upon chemisorption.

DOI: 10.1103/PhysRevB.76.195425 PACS number(s): 68.43.−h, 68.43.Bc, 73.20.Hb

I. INTRODUCTION

Carbon dioxide chemistry is of wide technological interest in both homo- and heterogeneous catalytic processes. In particular, it is an essential ingredient of the methanol synthesis reaction ($CO_2+3H_2 \rightarrow CH_3OH+H_2O$) which is industrially performed on Cu-based catalysts. Recent experiments on a model catalyst have pointed out that Ni/Cu can be 60 times more active than pure Cu for this reaction.[1–3]

Although available techniques, both experimental and theoretical, do not allow the evolution of the catalyst and the whole reaction process to be followed in detail under standard temperature and pressure conditions, investigations performed on model systems for simplified reaction schemes can yield precious information about intermediate species, contributing to the understanding of the underlying mechanisms. Despite the importance of the subject, only little work has been performed up to now. Not only the origin of the promoting role of Ni is still obscure but, surprisingly, there is a lack of knowledge concerning even more basic questions, such as the CO_2 interaction with Ni and other transition metal surfaces. This is related to the fact that CO_2 adsorption hardly occurs on Cu low-index metal surfaces under ultrahigh vacuum (UHV) conditions. On the contrary, on Ni(110), a bound CO_2 state has been observed.[4,5] The adsorption configuration of CO_2 on Ni(110) has been the subject of previous experimental and theoretical studies. Carbon dioxide has several possible modes of coordination with the underlying surface: a pure carbon coordination, a pure oxygen coordination, or a mixed carbon-oxygen coordination.

By means of angle resolved ultraviolet photoelectron spectroscopy and high-resolution electron energy loss (HREELS) spectroscopy, Bartos *et al.* found that CO_2 adsorbs on Ni(110).[5] Data at 80 K are compatible with a physisorbed state of the linear, undistorted molecule, whereas at temperatures in the 110–230 K range, there are indications for the formation of a chemisorbed, bent, and negatively charged molecule. It has been proposed that coordination sites with C_{2v} symmetry are favored, although without strong direct evidence and not excluding other sites such as C_s sites. Illing *et al.*,[6] on the basis of x-ray photoelectron spectroscopy (XPS), near-edge x-ray absorption fine structure, and diffuse low-energy electron diffraction (LEED), confirmed the presence of both linear-physisorbed and bent-chemisorbed CO_2 molecules on Ni(110). They suggested that in the latter case, the most favored configuration has a C_{2v} symmetry, with the molecular plane perpendicular to the Ni surface, with O atoms closer than the C atom to the Ni surface (pure oxygen coordination), in a reversed "V" shape, in analogy to the formate (HCOO) case which is known to bind to Ni(110) with both oxygen atoms.

Very little theoretical works are present in the literature, mostly based on cluster models. Freund and Messmer[7] used *ab initio* valence bond cluster calculations. Among the different coordination geometries considered, they found that pure oxygen and mixed carbon-oxygen configurations are more favorable than pure carbon configurations and that the molecule-surface bonding is better represented by CO_2^- rather than the neutral molecule. In their work, however, the real surface structure of Ni was not taken into account. Choe *et al.*[8] performed molecular orbital cluster calculations for modeling the CO_2/Ni(111) system and obtained a more favorable pure oxygen symmetric adsorption configuration. Recently, *ab initio* density functional theory (DFT) supercell calculations were successfully applied to numerous surface chemistry problems. Among the most relevant applications for the present study, we mention a recent detailed investigation of the interaction of CO with Ni(110).[9] Wang *et al.*[10] performed calculations for CO_2 on Ni(111), (100), and (110). At variance with previous indications in literature, they found that in the most favorable geometry, CO_2 occupies a hollow site and binds with Ni in an asymmetric way, with C closer to the surface and oxygen pointing upward, resulting in a molecular plane inclined with respect to the surface.

In summary, all experimental and theoretical data agree in relating CO_2 chemisorption with the formation of CO_2^-, a charged and bent species, which must therefore have a key role in the methanol synthesis.[11] However, it is not yet clear which is the most favorable adsorption geometry or whether there are different possible configurations and how their occupation does depend on coverage and temperature.

With the aim of clarifying these issues, we present here a combined experimental and theoretical investigation to characterize the CO_2 adsorption on Ni(110) in terms of energetics and vibrational properties by cross correlating XPS, temperature-programmed desorption (TPD), and HREELS data with spin-polarized pseudopotential DFT calculations of total energy, atomic forces, and dynamical matrices. We choose TPD and XPS in order to identify and quantify the different adsorbed species and their temperature behavior. In addition, by means of high-energy resolution vibrational spectroscopy, we investigate the nature of the molecule-surface bond, so to obtain a multiapproach complementary set of information.

Our experimental and theoretical findings indicate two energetically most favored adsorption sites and support the preferential binding of CO_2 with Ni through C rather than O atoms, thus confirming the predictions of Wang *et al.*[10] and pointing out a remarkable difference between CO_2 and HCOO.

II. EXPERIMENTAL SETUP

Experiments were carried out in two different UHV chambers. XPS and TPD analyses were performed in a multipurpose apparatus with a base pressure of 5×10^{-11} mbar equipped with LEED and spot profile analysis (SPA)-LEED optics, residual gas analyzer for TPD measurements, a conventional Mg K_α x-ray source ($h\nu=1253.6$ eV, $\Delta E=0.9$ eV), a monochromatic Al K_α source, and a VG MKII hemispheric electron energy analyzer. The sample was mounted on a four degrees of freedom manipulator, resistively heated, and cooled down to 90 K by liquid nitrogen. HREELS experiments were instead carried out in a dedicated chamber with a base pressure of 1.5×10^{-10} mbar, additionally equipped with a commercial LEED optics (OCI), a XPS facility (ESCA Omicron), and a EELS spectrometer (SPECS). Here, the sample was heated by both electron bombardment and irradiation from a tungsten filament, while cooling was per-

formed by liquid nitrogen. HREELS spectra were recorded in specular configurations, with a primary electron energy of 3.0 eV and an incidence angle of 62°. In order to maximize the signal from the low reflectivity, disordered CO_2 layer, the instrument was operated at resolution around 5 meV. Two distinct Ni(110) samples were used for the XPS-TPD and EELS experiments. The surface was cleaned by several cycles of ion bombardment ($Ar^+, E_k=3$ keV) and subsequent progressive annealing up to 1300 K. Oxidation cycles were performed periodically to remove carbon contamination. Surface order and cleanliness were checked by LEED and XPS, respectively.

III. THEORETICAL APPROACH

Our theoretical approach was based on the state-of-the-art spin-polarized DFT[12] as implemented in the PWSCF code of the QUANTUM ESPRESSO distribution.[13] We used the generalized gradient approximation (GGA) for the exchange and correlation (XC) term in the Perdew-Burke-Ernzerhof implementation[14] and we performed for comparison some tests with the local density approximation (LDA).[15]

Ultrasoft pseudopotentials from the publicly available repository of the QUANTUM ESPRESSO distribution have been used.[16] The valence electronic wave functions were expanded by a plane wave basis set with a kinetic energy cutoff of 24 Ry (convergence tests with 32 Ry). The Brillouin zone integration was carried out with smearing techniques[17] using an $8\times8\times8$ k-point mesh for bulk Ni (fcc) and corresponding meshes for slab supercells and an energy broadening of 0.01 Ry.

For bulk Ni, the GGA equilibrium lattice constant is equal to 3.52 Å, the bulk modulus 1.92 Mbar, and the magnetic moment $0.59\mu_B$, in standard good agreement with the corresponding experimental values of 3.52 Å, 1.86 Mbar, and $0.61\mu_B$, respectively.[18] LDA calculations give instead 3.42 Å for the lattice constant and 2.50 Mbar for the bulk modulus, thus giving an overbinding effect, as often occurs. The magnetic moment obtained by LDA, $0.57\mu_B$, is however in rather good agreement with experiments. The GGA bond length in free CO_2 is 1.172 Å (LDA, 1.166 Å), to be compared with the experimental value of 1.162 Å.[19]

Surfaces were described as extended systems using periodically repeated supercells with a slab geometry. Slabs containing an odd number of (110) atomic layers and CO_2 molecules symmetrically placed on each side of the slab allow to take advantage of the reflection symmetry of the system to reduce the number of k points for Brillouin integration; alternatively, describing the slab with a molecule adsorbed on a single side avoids the spurious interaction between the molecules adsorbed on the two sides of the slab but a dipole correction is needed.[20,21] We performed calculations using symmetric slabs; we checked that "single side" calculations with proper dipole corrections give similar results.

For the adsorbed geometries, most calculations were performed using supercells with in-plane (3×2) periodicity, corresponding to a CO_2 coverage of 1/6 ML (monolayer) when one molecule per side is contained in the supercell.[22] A $4\times4\times1$ k-point mesh is used with the (3×2) supercell. Tests with other coverage values and supercell in-plane periodicities were also performed in order to investigate the effect of lateral intermolecular interactions. Coverages of 1/4 and 1/2 ML are realized with (2×2) and (2×1) supercells and corresponding $4\times3\times1$ and $4\times6\times1$ k-point meshes, respectively, for Brillouin zone integration.

The adsorption energy per CO_2 molecule was calculated as

$$E_{ads} = 1/2\{E(CO_2/\text{slab}/CO_2) - [2E(CO_2) + E(\text{slab})]\}, \quad (1)$$

in the case of double-side configurations (a similar expression, but without the factors 1/2 and 2, applies in the case of single side calculations), where the first term is the total energy of the adsorbed system, the second is the total energy of free CO_2, and the third one is the total energy of the bare Ni slab. A negative E_{ads} indicates that the molecule is bonded to the surface and the comparison of the different energy values provides information concerning the relative stability of different adsorption sites.

Adsorption energies are rather sensitive to the slab thickness: $|E_{ads}|$ is about 0.1 eV higher for a double-side configuration with a Ni slab of nine layers with respect to the calculation performed using a five-layer slab. Adsorption energies are also affected by the choice of the XC functional: GGA, in particular, has been often found to underestimate binding energies, at variance with LDA, which typically gives a strong overbinding. Most of the calculations were performed with a Ni slab thickness of five layers and a vacuum space of 15 Å. We should attribute to the adsorption energies calculated with a double-side five-layer supercell a numerical error of $\approx\pm0.1$ eV mainly due to size effects. However, *differences* between the adsorption energies on the various possible adsorption sites are already converged within ≈0.02 eV for double-side five-layer configurations.

Several adsorption configurations were considered, starting from those with C_{2v} and C_s symmetries on high symmetry sites suggested in literature[5] to include others obtained by relaxing the symmetry constraint, since adsorbed CO_2 was not expected to have the same coordination of formate due to the very different electronic structure of the two molecules. Unconstrained optimization of atomic positions was applied to the CO_2 molecule and the first two surface Ni layers, which were allowed to relax until atomic forces were smaller than 1 mRy a.u.$^{-1}$ and the total energy was minimized.

Information about the chemisorption kinetics was obtained by studying various possible reaction pathways and energy barriers characterizing the chemisorption of single CO_2 molecules on the Ni surface. To this purpose, we used a recently proposed variant of the "nudged elastic band" method,[23] i.e., the "climbing image nudged elastic band" method,[24] which has proven to be a very efficient technique to determine minimum energy paths in complex chemical reactions.

Löwdin population analysis,[25] by projecting Bloch wave functions onto linear combinations of spin-resolved atomic orbitals, was used to obtain information about the atomic magnetic moments and charges.

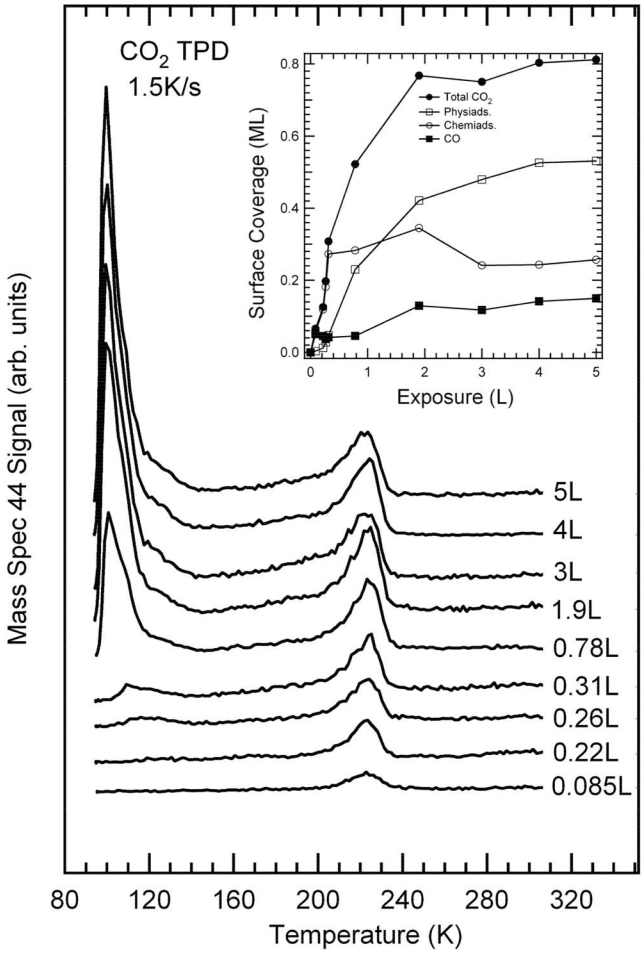

FIG. 1. TPD spectra obtained on Ni(110) as a function of the initial CO_2 exposure at 90 K. In the inset, a plot of the total and relative CO_2 desorbing coverage is shown, together with a quantification of the formed CO. The latter concentration is calculated via a cross-link between the TPD and the XPS data.

IV. EXPERIMENTAL RESULTS

A. Temperature-programmed desorption data

Figure 1 shows the mass 44 TPD spectra obtained as a function of the initial CO_2 exposure at 90 K and with a linear temperature ramp of 1.5 K/s. CO was also detected as a desorption product due to the dissociation of carbon dioxide into carbon monoxide and atomic oxygen (data not shown). For exposures above 0.3 L (1 L$=10^{-6}$ Torr s), two distinct mass 44 peaks are observed at 100 and 220 K, respectively. The low-temperature feature is due to the desorption of the CO_2 physisorbed multilayer, while the higher temperature peak is related to chemisorbed CO_2. Desorption from the low-temperature state takes place immediately with heating, thus indicating that its population is limited by the adsorption temperature. Chemisorbed CO_2, on the contrary, is stable on the surface up to $\approx$220 K. At this temperature, it partially desorbs and partially dissociates into CO and oxygen, both remaining as chemisorbed species on the surface, as suggested by XPS data discussed below. CO leaves the surface at temperatures between 370 and 450 K. Instead, atomic oxygen does not desorb, as corroborated by LEED patterns, which suggest the formation of the (3×1)-O ordered structure already at 365 K. CO and O recombination does not take place on this surface at the present conditions. For exposures lower than 0.3 L, physisorbed CO_2 is absent. Assuming a first order desorption process and a trial standard preexponential factor of 10^{13} s^{-1}, the estimated desorption energies from the features at 222 and 100 K are $\approx$0.60$\pm$0.15 and $\approx$0.26$\pm$0.05 eV for the chemisorbed and physisorbed-multilayer species, respectively.

TABLE I. Desorption temperature and core level binding energies for different species identified in the XPS analysis after exposure of the clean surface to 4 L of CO_2 at 90 K.

	Desorption T (K)	O 1s (eV)	C 1s (eV)
Chemis. CO_2	220	530.6	286.2
Physis. CO_2	100	534.0	290.6
Oxygen		529.3	
CO	415	531.0	285.1

In order to properly describe the desorption of the physisorbed layer, many possible processes should be considered, including zero and fractional order kinetics. A deeper investigation of this issue is beyond our purposes. So, just for the sake of simplicity, we approximately assume a classic molecular desorption process (first order) to give a rough hint about the enrolled desorption energies for the multilayer.

In the inset of Fig. 1, we plot the total CO_2, chemisorbed and multilayer, plus the formed CO coverage obtained from the TPD measurements with a cross-link to the XPS peak areas. It can be observed that the coverage of carbon monoxide which forms upon CO_2 decomposition grows up to about 2 L exposure, i.e., well beyond the chemisorbed CO_2 saturation yield. This indicates that conversion from the multilayer CO_2 to the chemisorbed species may occur during the heating process.

B. X-ray photoelectron spectroscopy data

XPS data (see Table I and Fig. 2) confirm the findings of TPD analysis. O 1s and C 1s core level spectra were collected as a function of the annealing temperature after exposure of the clean surface to 4 L of CO_2 at 90 K. The O 1s spectra at 90 K consist of two well separated peaks with binding energies of 534.0 and 530.6 eV, which can be attributed, on the basis of previous analysis,[6] to physisorbed and chemisorbed CO_2 species, respectively. The feature at high binding energy disappears after annealing to 150 K in agreement with TPD data, thus suggesting that the physisorbed CO_2 state is not stable on the surface at this temperature. Moreover, a new O 1s component, corresponding to CO, appears at 531.0 eV. In addition to the CO related signal, above 365 K, a new peak grows at a binding energy of 529.3 eV, which is associated with atomic oxygen produced by CO_2 dissociation. After annealing to 500 K, the spectra show only the contribution of the adsorbed atomic oxygen species.

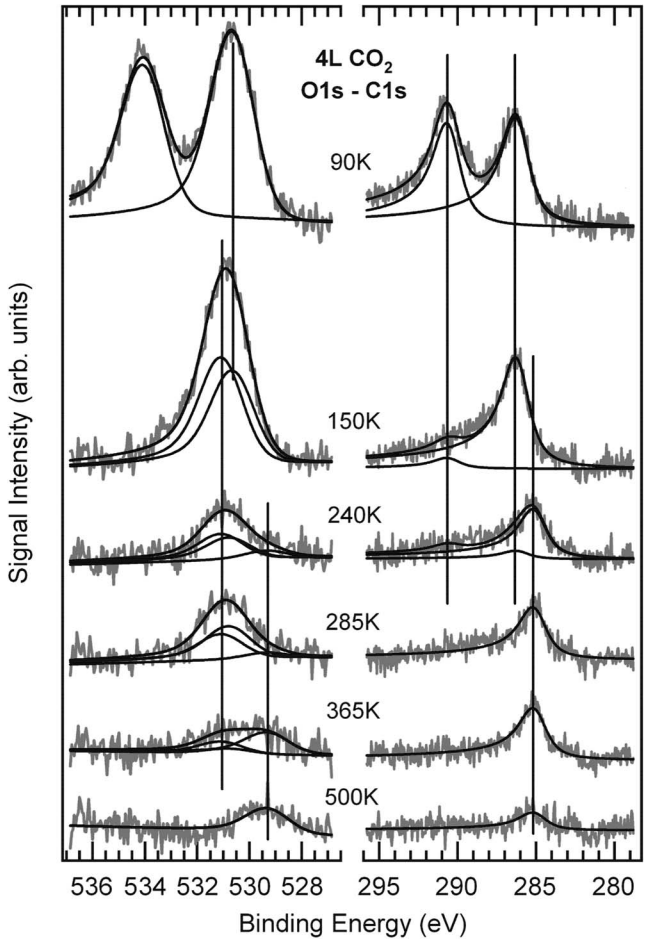

FIG. 2. Oxygen 1*s* (left) and carbon 1*s* (right) XPS core level spectra ($h\nu$=1253.6 eV) upon exposure of the Ni(110) surface to 4 L of CO_2 at 90 K and subsequent stepwise annealing.

For the C 1*s* spectra, the temperature behavior of the different species is similar. At 90 K, the spectra show two components at 290.6 and 286.2 eV, attributed to physically and chemically bound CO_2, respectively. A single contribution at 285.1 eV is present in the spectra after annealing between 240 and 500 K, thus in agreement with the carbon monoxide behavior for this system.

C. High-resolution electron energy loss spectroscopy data

HREELS spectra, shown in Fig. 3, upper panel, were collected as a function of the initial CO_2 exposure at 87 K. Already after a dose of 0.01 L, several losses can be resolved in the spectra at 46, 81, 90, 141, and 168 meV. Their intensity grows with exposure to CO_2. Above 0.02 L, a new feature appears at 290 meV, while a contribution at 128 meV can be distinguished for doses larger than 0.11 L. In the 200–250 meV range, small contributions due to water and CO contamination are present in the loss spectra due to adsorption from the background during the acquisition time and to carbon dioxide dissociation at defect sites, respectively.

Figure 3, lower panel, reports HREELS spectra of Ni(110) exposed to 0.22 L of CO_2 at 87 K and subsequently heated

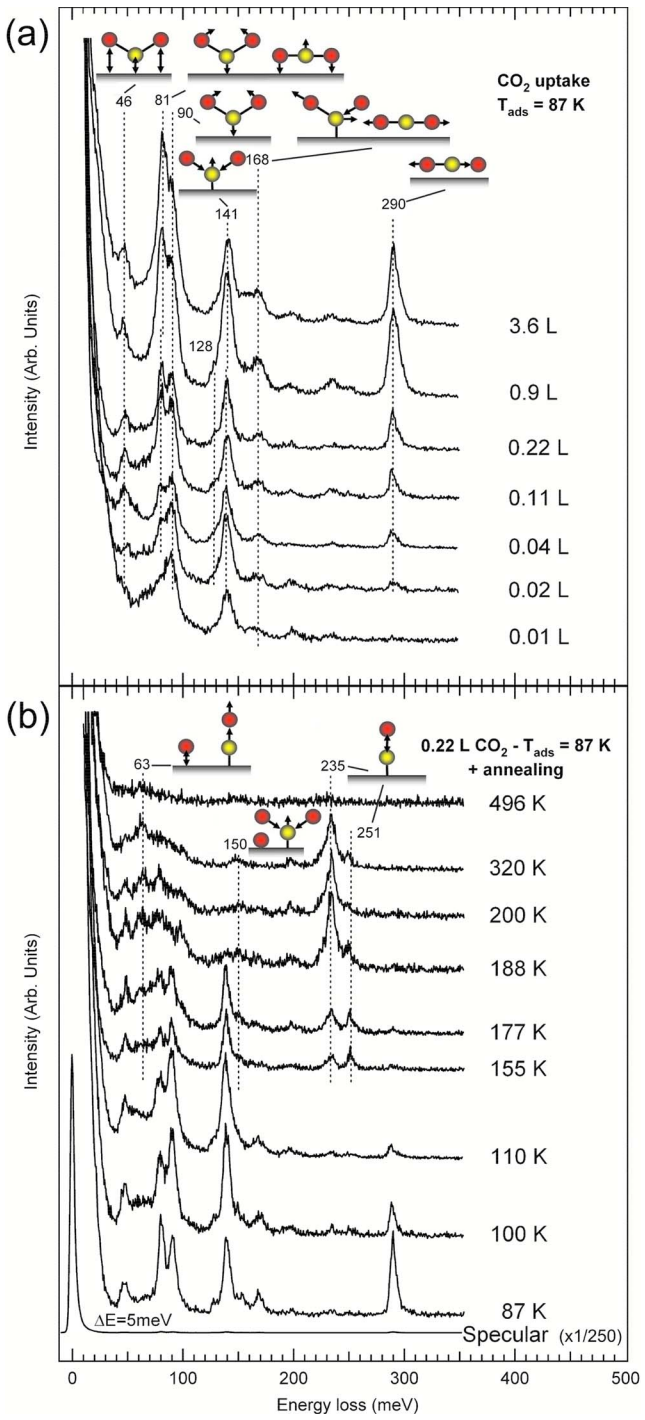

FIG. 3. (Color online) HREELS spectra on Ni(110) (a) as a function of the initial CO_2 exposure at 87 K (CO_2 uptake, upper panel) and (b) of the surface initially exposed to 0.22 L of CO_2 at 87 K and subsequently heated to different temperatures (CO_2 annealing, lower panel).

to increasing temperatures. Below 100 K, there are six prominent losses at 48, 80, 90, 140, 168, and 290 meV. Furthermore, two shoulders of the 140 meV peak are present around 128 and 150 meV. For increasing temperature, the high frequency peak at 290 meV decreases in intensity and completely disappears above 110 K, while the other losses still persist. According to TPD and XPS data, as well as to

previous results,[5,26] it is reasonable to associate this component to physically bound CO_2. We postpone the discussion of the other losses to the following sections. It is interesting to observe the intensity behavior of the 80 and 90 meV peaks as a function of the temperature. Markedly, the annealing to 100 and 110 K leads to a reduction of the 80 meV signal, while the 90 meV loss seems not to be affected, remaining as intense as the 141 meV loss. At 155 and 177 K, both losses show almost the same intensity. At these temperatures, the peak assigned to physisorbed CO_2 disappears. Above 155 K, the intensity of the loss at 140 meV decreases and goes to zero at 188 K. Spectra in the 155–320 K range show also additional peaks at 63, 150, 235, and 251 meV. After annealing to 320 K, the peaks attributed to chemisorbed CO_2 disappear, while the new vibrational frequencies are still present. On the basis of the TPD and XPS results, it is known that CO_2 dissociation into CO and oxygen occurs. The low intensity loss at 150 meV could be associated with the CO_2 symmetric stretching mode influenced by the coadsorption of oxygen due to the already dissociated molecules.[26]

CO remains on the surface beyond 320 K. The losses at 235 and 251 meV are in agreement with the observed CO behavior in previous studies.[27,29] Notably, the relative intensities of these signals change with temperature. Above 177 K, the 251 meV peak decreases in favor of the 235 meV peak. The two losses are due to two different coordination sites, namely, bridge and on-top sites, according to literature.[27,29] The population of the two different adsorption sites for CO is a function of the total surface coverage, which changes with surface temperature due to the different competing mechanisms of CO_2 dissociation, CO_2 desorption, and CO desorption. At 500 K, a single dominant peak is observed at 63 meV: it is attributed to the atomic oxygen produced by the CO_2 dissociation process.[26]

The variation of the work function ϕ of the Ni(110) surface upon CO_2 adsorption has been studied in Ref. 5. At low temperature (80 K), it increases with coverage at first by about 0.6 eV, then decreases, while at high temperature (140 K), it has a higher increment (about 0.9 eV) and remains constant after a certain coverage. At higher temperature (200 K), the increase is higher ($\approx$1.0 eV).

On the basis of our photoemission and HREEL experiments, the previously found work function changes are explained, suggesting the involvement of two different species giving opposite contributions to the work function.[4,5] In Fig. 4, we show the relative coverage of physisorbed and chemisorbed CO_2 species as a function of total surface coverage at low temperature. Quantitative data about the surface coverage of the two chemically inequivalent adsorbed CO_2 species were obtained by cross correlating CO and CO_2 XPS data with the TPD series obtained as a function of the CO_2 exposure. In the same figure, we also report previous work function data from Ref. 5 in the same low-temperature conditions. At low coverage, the chemically bound CO_2, which is the only adsorbate present on the surface, causes the initial rise. On the contrary, the physisorbed CO_2 gives a negative contribution to the work function, thus yielding a slowdown in the initial increase. When the coverage of both species reaches the same value (about 0.3 ML), the work function goes through a maximum. This is due to the fact that above this value, only the coverage of the physisorbed species increases, while a saturation coverage is found for the chemisorbed CO_2 species.

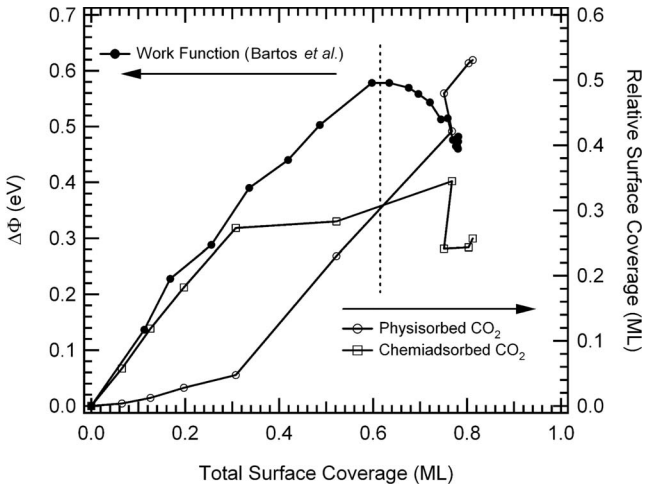

FIG. 4. Relative surface coverage (right scale) of the physisorbed and chemisorbed CO_2 species as a function of the total surface coverage, obtained by cross-linking CO and CO_2 XPS data with the TPD series obtained as a function of the CO_2 exposure at low temperature. Data for work function variation in the same low-temperature conditions from Bartos (Ref. 5) are also reported (left scale).

V. THEORETICAL RESULTS

A. Structure, energetics, and electronic properties

The adsorption geometries compatible with the constraint of C_{2v} or C_s symmetry, as suggested from previous literature,[5,6] include different adsorption sites for C, namely, *short-bridge* (SB), *long-bridge, on-top, and hollow* sites, with the molecular plane perpendicular to the surface and parallel either to the $[1\bar{1}0]$ or to the [001] directions. Among them, we found that the favored adsorption geometries are a pure carbon SB with C_{2v} symmetry (hereafter indicated with SB-C_{2v}) and a C_s configuration where C sits almost on a SB site but with a mixed carbon-oxygen coordination, which makes the molecule asymmetric with respect to the surface (hereafter indicated with SB-C_s), as shown in Fig. 5. Apart from symmetry, the two configurations are hardly distinguishable in terms of structural parameters and energetics: the SB-C_{2v} adsorption energy in the double-side nine-layer (3×2) supercell using GGA is -0.26 eV/CO_2 molecule, and differences with the SB-C_s are within 0.02 eV. Likely, SB-C_{2v} is an intermediate state between two specular SB-C_s coordination patterns. In the following, we will not distinguish the two, unless explicitly stated.

The most stable configuration, however, turns out to be very similar to the one reported by Wang *et al.*,[10] i.e., with C almost in the hollow site, with a dominant carbon coordination with Ni and oxygen atoms pointing upward and the molecular plane inclined with respect to the Ni surface normal (hereafter indicated as *hollow-up* (HU) configuration, also shown in Fig. 5). In the double side nine-layer (3×2)

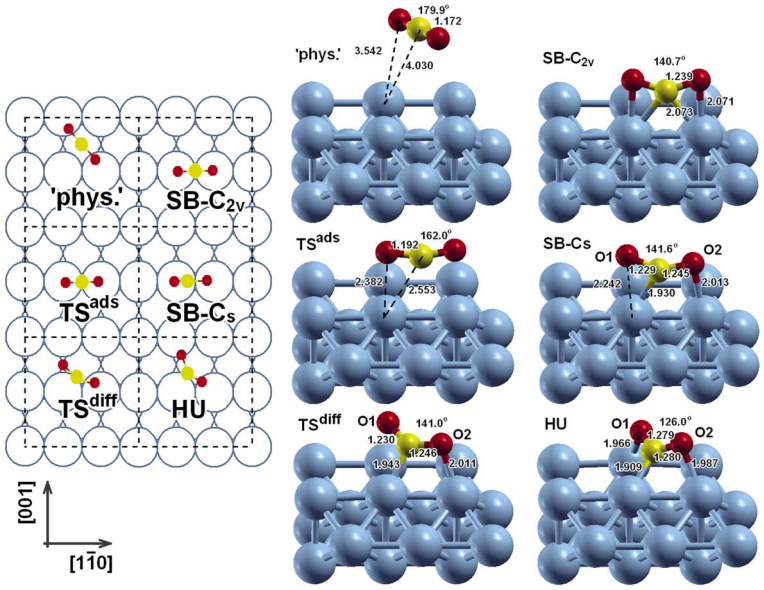

FIG. 5. (Color online) Geometries of CO_2 adsorbed on different sites on Ni(110) surface [short bridge (SB-C_{2v} and SB-C_s) and hollow up (HU)], transition states along the gas phase→SB path and along the SB↔HU diffusion path (TS^{ads} and TS^{diff}), and linear weakly bound ("phys.") configuration (see text). Left panel, schematic top view of the (3×2) cell; right panels, ball and stick models generated using XCRYSDEN (Ref. 40). Distances are in Å.

supercell, this corresponds to an adsorption energy of −0.32 eV/CO_2 molecule in GGA. Calculations performed with a double-side five-layer supercell give E_{ads}=−0.17 and −0.24 eV for SB and HU, respectively. As already discussed in Sec. III, adsorption energies are rather sensitive to the slab thickness, while energy differences are already converged within ≈0.02 eV for a double-side five-layer slab. As an example, the calculated binding energy differences between the HU and SB configurations are 0.07, 0.08, 0.06, and 0.06 eV in the case of 5-, 7-, 9-, and 11-layer slabs, respectively. The small difference of ≈0.07 eV/CO_2 molecule between HU and SB configurations makes both compatible with the experimental results.

Structural details of the adsorption configurations are indicated in Fig. 5: the O-C-O angles are 140° and ≈126° and the C-O bond lengths elongate up to 1.28 and 1.23 Å in SB and HU, respectively. The weakly chemisorbed CO_2 induces only very small rearrangements of surface Ni atoms.

The adsorption energy depends on coverage: due to lateral intermolecular repulsive interactions, its absolute value decreases for increasing coverage until saturation. Tests performed in GGA with a double-side five-layer supercell give adsorption energies equal to −0.22, +0.04 eV for HU and −0.05, −0.05 eV for SB at 1/4 and 1/2 ML coverages, respectively. This trend suggests a saturation coverage between 1/4 and 1/2 ML, consistent with the experimental findings of about 0.3 ML (see Fig. 4).

The general trend of LDA overbinding is confirmed by the fact that CO_2/Ni(110) adsorption energies of the order of 1 eV higher than GGA are predicted. Remarkably, the relative stability and the structural configurations of the different adsorption geometries are almost the same in GGA and LDA, thus reinforcing the GGA results.

In general, DFT does not properly account for the van der Waals (vdW) forces which are responsible for weakly bound atomic and/or molecular physisorbed states on surfaces (see Sec. VI). However, both GGA and LDA calculations predict a weakly bound, metastable state, where the undistorted CO_2 molecule floats at about 3.4 Å (2.3 Å) in GGA (LDA) from the Ni surface, with its axis almost parallel to it and an adsorption energy of −0.07 eV. This state is only an indication of the existence of a physisorbed state.

Both HU and SB chemisorbed geometries are characterized by a sizable electron transfer from surface to CO_2, as it can be estimated by calculating the atomic Löwdin charges (see Table II): the total charge transfers from the substrate to the molecule are 0.93, 0.64, and 0.62 electrons for the HU, SB-C_{2v}, and SB-C_s configurations, respectively, as obtained by GGA for 1/6 ML coverage, with an estimated error

TABLE II. Atomic charges (in units of $|e|$) in the isolated, free-standing, neutral, and linear CO_2 molecule (first row) and related variations in the adsorbed geometries and transition states (last part of the table). The variations in the neutral free molecule positioned in the same bent geometry of the adsorbed configurations are reported in the central part of the table for comparison. Results are calculated by GGA for 1/6 ML coverage. Different columns refer to the carbon atom, the two oxygen atoms (which are different in HU, SB-C_s, and TS geometries), and the total CO_2 molecule.

Configuration	C	O1	O2	CO_2
Isolated, free standing				
	+0.58	−0.29	−0.29	0
Variation in free CO_2, neutral but in the adsorbed geom.				
SB-C_{2v}	−0.06	+0.03	+0.03	0
SB-C_s	−0.06	+0.04	+0.02	0
HU	−0.10	+0.05	+0.05	0
Variation in adsorbed and transition states				
SB-C_{2v}	−0.41	−0.11	−0.11	−0.64
SB-C_s	−0.40	−0.08	−0.14	−0.62
HU	−0.53	−0.21	−0.19	−0.93
TS^{ads}	−0.15	−0.03	−0.02	−0.19
TS^{diff}	−0.42	−0.08	−0.19	−0.69

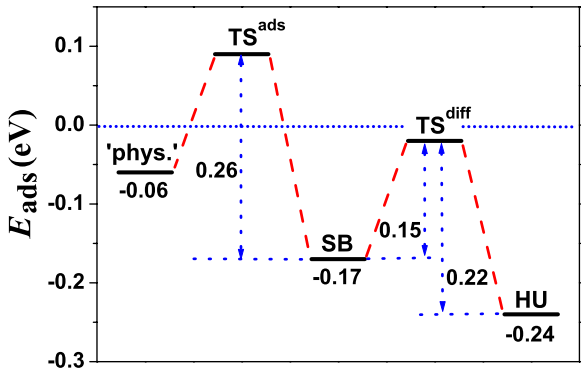

FIG. 6. (Color online) Energy diagram for different CO_2 adsorption sites on Ni(110) and relative barriers. The data reported are obtained from GGA double-side five-layer supercell calculations. The zero of the energy is set to the nondissociated molecule at infinite distance from the surface.

of ±0.05 electrons due to the projection procedure. Table II also shows that a neutral free CO_2 molecule positioned in the same bent geometry of the adsorbed configuration is polarized with electrons mainly localized on the oxygen atoms, thus resulting in a net dipole. Extra electrons on the adsorbed molecule come from the Ni atoms close to CO_2; charge density plots (not shown here) indicate that most of the transferred electrons localize between C and Ni atoms. It is interesting to notice the relationship between the charge, structure, and strength of the chemical bond which occurs also in the gas phase: free CO_2^- assumes spontaneously a bent configuration with the O-C-O angle of about 133° and a weaker C-O bond elongated from 1.16 to 1.22 Å.[28] Finally, we observe that the estimated charge transfer in LDA is qualitatively the same than in GGA, but about 10% larger, consistent with the overbinding between the molecule and surface.

The spin-resolved Löwdin charge analysis allows us also to study the surface magnetization: whereas at the clean surface the magnetic moments of the outermost Ni atoms are enhanced with respect to the bulk, CO_2 chemisorption induces a reduction of the surface magnetic moment compared to the clean surface. We address the reader to Ref. 30 for further details.

We investigate the CO_2 adsorption path on Ni from a linear, neutral configuration far away from the surface: for the sake of definiteness, we start from the metastable weakly bound state at 3.4 Å from the surface. We study also the diffusion paths between different adsorption configurations, namely, HU↔SB-C_{2v} or SB-C_s. The geometries of the transition states along the adsorption path on SB (TS^{ads}) and along the diffusion path SB↔HU (TS^{diff}) are shown in Fig. 5. The energies obtained with a double-side five-layer supercell are summarized in the diagram shown in Fig. 6, where the relevant energy barriers along those paths are indicated. SB-C_{2v} and SB-C_s configurations are not distinguished since they differ by only ≈0.02 eV, which is the relative numerical accuracy of the adsorption energy. The diffusion barrier SB→HU of ≈0.15 eV indicates that both HU and SB sites can be populated at ≈90 K. Our calculations predict that a multistep adsorption path *gas phase*→SB→HU is the most favorable for the adsorption process in the HU site with a small activation barrier of about 0.1 eV given by the energy [Eq. (1)] of TS^{ads}; in the inverse path, the desorption barrier from the SB site is 0.26 eV. Other paths are characterized by higher barriers. We attribute to these energy barriers a numerical error of the same order of the one affecting the adsorption energies, i.e., ±0.1 eV.

TABLE III. Work function variation $\Delta\phi$ (in eV) with respect to the clean Ni surface upon CO_2 adsorption. Two different adsorption sites as a function of the coverage are considered. Results from GGA (LDA) are reported.

Coverage (ML)	HU	SB-C_{2v}
1/6	+0.89 (0.84)	+0.65 (0.67)
1/4	+1.16 (1.17)	+0.83 (0.81)

The transition state TS^{ads} is characterized by sudden changes of the O-C-O bond angle (see Fig. 5) and charges (see Table II) with respect to the gas phase, indicating that *bending* and *electron transfer* are two important features in the chemisorption process.

B. Work function

We calculate the work function ϕ for the clean and CO_2 covered Ni(110) surface using both GGA and LDA. In slab model, the work function can be calculated as the energy difference between the Fermi energy and the electrostatic potential in the vacuum region. The latter is the sum of electronic Hartree, Coulomb, and XC potentials. Since the XC potential goes to zero rather slowly in the vacuum region, it is convenient to evaluate the vacuum level by simply neglecting the XC contributions.[31]

The GGA work function for the clean Ni surface is about 4.67 eV, in good agreement with the experimental value of 4.65 eV.[32] The LDA prediction is instead 4.97 eV. Our results for the work function variations $\Delta\phi$ upon CO_2 adsorption are listed in Table III for different coverages. Considering CO_2 adsorbed in SB or HU geometries, ϕ increases with coverage in both cases, with higher increment for HU than SB. Despite the few data reported in the table (even including the zero coverage, zero variation reference point), the work function seems to have a nonperfect linear behavior with coverage. This is explained by the coverage dependent interaction between neighboring adsorbed CO_2 molecules (with an estimated energy of about 0.01 and 0.07 per molecule at 1/6 and 1/4 coverages) that also affect the molecule-surface interaction. The LDA gives for all cases higher ϕ values than GGA, but the relative variation $\Delta\phi$ with respect to the clean surface is similar.

Charge and bending of the chemisorbed CO_2 molecule give a simple rationale for the work function increase upon chemisorption: (i) the electron transfer from the surface to the molecule creates an additional surface dipole, with the same orientation of the dipole due to the electron spill out from the clean surface; (ii) the bent molecule, even if neutral,

TABLE IV. Work function variation $\Delta\phi$ and the three relative contributions indicated in the text for CO_2 in different adsorption configurations for 1/6 ML coverage. All data are in eV.

	$\Delta\phi$	$\Delta\phi_{surf}$	$\Delta\phi_{mol}$	$\Delta\phi_{elec}$
HU	0.89	−0.01	0.49	0.41
SB-C_{2v}	0.65	−0.01	0.53	0.13
SB-C_s	0.75	−0.01	0.51	0.25

has an intrinsic dipole pointing from the oxygen atoms to the carbon atom (see central part of Table II) and thence toward the surface in the case of a pure carbon or a mixed oxygen-carbon coordination, again in the same direction of the intrinsic surface dipole. In a more refined analysis of the work function change, we could quantitatively distinguish three different contributions,

$$\Delta\phi = \Delta\phi_{elec} + \Delta\phi_{mol} + \Delta\phi_{surf}, \tag{2}$$

where the first two are those discussed above and $\Delta\phi_{surf}$ is related to the surface structural changes induced by the presence of the molecule. $\Delta\phi$, $\Delta\phi_{mol}$, and $\Delta\phi_{surf}$ can be obtained by direct calculations and $\Delta\phi_{elec}$ by difference.

As reported in Table IV for the 1/6 ML coverage with GGA approximation, $\Delta\phi_{mol}$ is the largest contribution to $\Delta\phi$: this is a strong argument in favor of a pure carbon or a mixed oxygen-carbon coordination with the surface rather than a pure oxygen coordination to explain the experimentally observed increase of the work function upon chemisorption.

The increment of the work function predicted both by GGA and LDA is rather high with respect to the observed values at low temperature:[5] for instance, at a total coverage of 1/6 ML, where almost only chemisorbed species are present in the experiment, the observed increment at low T is about 0.2 eV, whereas the calculated one is in the 0.6–0.9 eV range depending on whether SB or HU sites are occupied.

We note that a much higher increment in the work function, as large as 1 eV, has been experimentally observed at higher T, which might be consistent with our calculated results. A quantitative comparison is however, not possible: in the original data, the observed work function change is related to the CO_2 exposure, rather than the CO_2 coverage.

We argue, however, that DFT overestimates the work function, predicting a larger electron transfer that enhances both $\Delta\phi$ and $\Delta\phi_{mol}$. We further discuss this point in Sec. VI.

We are not able to quantitatively explain the experimentally observed decrease of the work function for coverages higher than ≈0.6 ML, when chemisorbed and physisorbed species should be almost equally present on the surface. We argue that the physisorbed multilayer could induce strong polarization effects, acting in the opposite direction of the intrinsic surface dipole and thus reducing ϕ. We cannot address further this issue here, not only for the size of the model system needed to properly take into account the coexistence of both chemisorbed and physisorbed species but also due to the intrinsic limitations of the DFT approach that does not describe correctly the polarization effects between weakly bound objects. For completeness, we only report that our tests on linear neutral molecules at about 3.4 Å from the surface indicate that they have a negligible effect on the work function of the bare Ni surface.

C. Vibrational frequencies

Vibrational modes and frequencies were calculated within DFT according to the approach described in Ref. 33. The dynamical matrix was constructed from the forces due to independent off-equilibrium displacements of C, O, and the first layer Ni atoms.

As a benchmark, the three normal vibration modes of linear, neutral, and free CO_2 were calculated within GGA and found equal to 80, 160, and 288 meV for the bending, the symmetric stretching, and the asymmetric stretching modes, in good agreement with the experimental values for the gas phase of 83, 165, and 291 meV, respectively.[34] The slightly larger LDA values were within the numerical uncertainty, ±2 meV.

Table V summarizes the vibrational frequencies of CO_2/Ni(110) calculated with GGA (the lower values of the intervals reported) and LDA (upper values).

In the case of SB, both C_s and C_{2v} symmetries are included in the reported ranges. The differences between GGA and LDA values for the internal CO_2 modes are compatible

TABLE V. Vibrational frequencies (in meV) for CO_2 in different chemisorption configurations (HU and SB) and in the weakly bound, linear, and neutral state described in the text. Ranges indicate estimates calculated with GGA (typically the lower limit) and LDA (upper limit). In the case of SB, both C_s and C_{2v} symmetries are included in the reported range. The experimental values tentatively attributed to the different modes are shown in italics.

Mode	HU	*Expt.*	SB	*Expt.*	Linear	*Expt.*
Asymm. stretching	173–175	*168*	216–219		287	*290*
Symm. stretching	136–140	*141*	140–144	*141*	160	*168*
Bending	88–91	*90*	80–83	*81*	79	*81*
Hindered rotation (out of CO_2 plane)	50–53		63–64		78	
External stretching	44–52	*46*	39–49	*46*	25	
Hindered rotation (in CO_2 plane)	41–42		29–40		25	

with the numerical accuracy, whereas larger differences (≈8–10 meV) are found for the external stretching and hindered rotation (in the CO_2 plane) modes involving directly the interaction with the substrate. Most of the modes are characterized by very similar frequencies in HU and SB chemisorbed configurations; differences between HU and SB clearly beyond the numerical uncertainty are found for the asymmetric stretching mode (≈40 meV) and, to a less extent, for the bending mode (≈10 meV).

The configuration with linear, neutral, and weakly bound CO_2, far apart from the surface, is characterized, as expected, by the same frequencies of the free molecule and the corresponding values can be unambiguously identified in the experimental HREELS spectra (last two colums of Table V).

Besides the peaks corresponding to physisorbed CO_2, also almost all of the other peaks of the HREELS spectra can be attributed to one particular mode of chemisorbed CO_2. The peak at 46 meV is compatible with the external stretching mode for HU and SB and similarly the peak at 141 meV corresponds to a symmetric stretching for the same configurations. We can attribute the 90 meV peak to the bending mode of HU and the 81 meV peak to the one of SB, besides the physisorbed molecule. This is one of the most interesting results emerging from the comparison of experimental and theoretical data since from the HREELS spectra upon annealing, it is clear that the 81 meV peak is still present well above 110 K, whereas the peak at 290 meV characterizing the physisorbed species disappears: for instance, at 177 K, both the 81 and the 90 meV peaks are well distinguishable, thus suggesting the presence of two different chemisorbed species, namely HU and SB.

The peak at 168 meV, besides the physisorbed CO_2, could also correspond to the asymmetric stretching mode of HU. The asymmetric stretching modes for the different chemisorption sites are characterized by a dipole moment almost parallel to the surface so that they are hardly visible using HREELS: this is likely the reason why the asymmetric stretching mode of SB, both C_s and C_{2v}, predicted to be around 216–219 meV, is not observed experimentally, while the asymmetric stretching mode of HU, which has a larger component perpendicular to the surface, is instead observed at 168 meV. This attribution is further corroborated by the fact that the intensity of the peak at 168 meV does not rescale with temperature like the peak at 290 meV, as we would expect if the peak was only due to the physisorbed CO_2.

The dramatic reduction of the asymmetric stretching frequency is related to the negative charge accommodated by the adsorbed CO_2: it is interesting to note that also in gas phase, the frequency of the asymmetric stretching mode strongly decreases from 290 to 207 meV from neutral CO_2 to ionized CO_2^-.[28]

Finally, we cannot find a straightforward explanation for the small peak detected at 128 meV present at the initial low temperature.

VI. DISCUSSION

Combined experimental and theoretical findings yield consistent indications about two inequivalent adsorption sites that can be simultaneously populated at low temperature. In the SB configuration, the molecular plane is perpendicular to the surface, while in the HU configuration, the molecular plane is inclined with respect to the surface. In both sites, the molecule has mainly pure carbon coordination with the metal and is negatively charged and bent.

This result has been obtained even though the CO_2 overlayer does not show any ordering, thus precluding the use of conventional experimental structural techniques (LEED, LEED I-V, and photoelectron diffraction). Consequently, the complete interpretation of the experimental data has been possible only with the corroboration of theoretical investigations. The application of the latter to this system, on the other side, is nontrivial due to the weakness of the molecule-surface interaction.

It is well known that standard functionals do not account for vdW forces (dispersion forces), which can be relevant in weakly bound configurations characterized by rather large molecule-surface separations. Interesting efforts toward the inclusion of long-range dispersion forces in DFT have been recently made.[36] In the present case, the interatomic distances involved in the chemisorbed configurations are short enough (carbon-Ni surface distance is of the order of 2 Å or less) to guarantee the predominance of electrostatic and covalent interactions over vdW forces. At variance, this is not the case for a possible physisorbed state, where the nature of the bonding is actually very weak.

In order to have a feeling of the reliability of our results based on standard functionals, we performed a few tests by calculating the vdW contribution to the adsorption energy on the basis of self-consistent charge density distribution following the approach proposed in Refs. 37 and 38. Our tests are limited to HU configuration in the non-spin-polarized case and therefore give us only some qualitative information. As expected for covalently bonded systems, we found that vdW corrections are not very important in chemisorbed configurations: they are at most ≈4% of the adsorption energy and, remarkably, do not influence the equilibrium geometries. From this test and from the comparison of LDA and GGA results, we can therefore conclude that the predicted equilibrium geometries and the relative stability of chemisorbed configurations are reliable. On the contrary, in weakly bound linear geometry, vdW corrections are much more important and can seriously affect the predicted equilibrium configuration.

Another delicate point in the application of DFT to problems of adsorption is the description of the interaction of the lowest unoccupied molecular orbital (LUMO) and highest occupied molecular orbital (HOMO) with the metal substrate, also in the case of chemisorption. Standard functionals could overestimate the interaction of the LUMO with the metal substrate, thus overestimating the metal-adsorbate charge transfer, as it probably occurs in the present case. This error is related to the *gap problem* of standard DFT. Better XC functionals could increase the HOMO-LUMO separation and correct the estimate of the charge transfer. The adsorption on a metal, moreover, can influence the molecular HOMO-LUMO gap through surface polarization effects which are absent in DFT. An *image potential* model accounting for these effects has been recently proposed for weakly

adsorbed systems such as benzene on graphite.[39]

Although the calculated charge transfer and work function changes are not precise, the qualitative results are reliable and the evidence that charge and bending are essential factors in the CO_2 chemisorption process on Ni(110) suggests some further considerations. The work function at Ni(110) is $\approx 0.2-0.3$ eV smaller than that at (001) and (111) surfaces. In general, only few cases of CO_2 chemisorption on clean metal surfaces are reported in literature, while many cases with pre- or coadsorbed alkali atoms are reported. This seems to suggest the following rationale: (i) stable adsorption geometries correspond to negatively charged CO_2; (ii) electron transfer from the surface to CO_2 is needed; (iii) the lower the work function of the metal surface, the easier the electron transfer and the CO_2 sticking and/or adsorption and the stronger the interaction between CO_2 and surface; (iv) alkali atoms on metal surfaces reduce the work function and promote the formation of a bent and negatively charged CO_2, which strongly interacts with the surface with a direct or indirect—surface mediated—electron transfer to the molecule. An example of alkali promoted adsorption of CO_2 on Pt(111) is reported for coadsorbed K atoms.[35]

VII. CONCLUSIONS

Combined experimental and theoretical investigations on CO_2 adsorption on Ni(110) have allowed us to identify two inequivalent chemisorption sites, SB and HU, which are simultaneously populated at low temperature, differing in energy by about 0.07 eV and with a diffusion barrier SB→HU of about 0.15 eV. GGA predicts a desorption barrier of 0.26 eV from the SB site and a favored multistep desorption process from HU through SB, compatible with the measured desorption energy.

A clear correspondence can be established between the calculated vibrational frequencies of the different chemisorbed configurations and the main peaks detected by HREELS. With the exception of the hindered rotation modes, which are not observable due to dipole scattering rules, all the other modes characterizing the adsorption geometries can be identified; in particular, the peak detected at about 168 meV, which is present in the spectra after 0.01 L of CO_2 in the absence of 290 meV feature, can be interpreted as a clear fingerprint of the presence of the HU configuration and attributed to its asymmetric stretching mode which is clearly different from the SB case.

Common features of all the chemisorbed geometries are (i) the activation barrier for the adsorption process, (ii) nonnegligible electronic charge transfers from the metal to the molecule, and (iii) bending of the molecule with C atom closest to the surface.

Our calculations agree qualitatively with previous results concerning the work function increase upon chemisorption.

The roles of charge and bending of the adsorbed CO_2 are discussed in detail to give a rationale concerning the work function changes reported in the literature and, in particular, as an argument in favor of a carbon or mixed oxygen-carbon coordination of the molecule with Ni.

ACKNOWLEDGMENTS

Computational resources have been partly obtained within the "Iniziativa Trasversale di Calcolo Parallelo" of the Italian *CNR-Istituto Nazionale per la Fisica della Materia* (CNR-INFM) and partly within the agreement between the University of Trieste and the Consorzio Interuniversitario CINECA (Italy). We acknowledge financial support from Sincrotrone Trieste SCpA, the Italian Ministry of University and Research through the projects FIRB (Grant No. RBNE0155X7), PRIN (Grant No. 2003023939), and FISR2002 ("Nanosistemi inorganici ed ibridi per lo sviluppo e l'innovazione di celle a combustibile"), and the Italian Interuniversity Consortium on Materials Science and Technology (INSTM). The Genova group acknowledges financial support from Compagnia S. Paolo. We thank Felipe H. Valencia for his help in estimating the van der Waals contribution to the adsorption energies and P. L. Silvestrelli for useful discussions.

[1] J. Nerlov and I. Chorkendorff, Catal. Lett. **54**, 171 (1998).
[2] J. Nerlov and I. Chorkendorff, J. Catal. **181**, 271 (1999).
[3] J. Nerlov, S. Sckerl, J. Wambach, and I. Chorkendorff, Appl. Catal., A **191**, 97 (2000).
[4] H.-J. Freund and M. W. Roberts, Surf. Sci. Rep. **25**, 225 (1996).
[5] B. Bartos, H.-J. Freund, H. Kuhlenbeck, M. Neumann, H. Lindner, and K. Müller, Surf. Sci. **179**, 59 (1987).
[6] G. Illing, D. Heskett, E. W. Plummer, H.-J. Freund, J. Somers, Th. Lindner, A. M. Bradshaw, U. Buskotte, M. Neumann, U. Starke, K. Heinz, P. L. de Andres, D. K. Saldin, and J. B. Pendry, Surf. Sci. **206**, 1 (1988).
[7] H.-J. Freund and R. P. Messmer, Surf. Sci. **172**, 1 (1986).
[8] S. J. Choe, H. J. Kang, D. H. Park, D. S. Huh, and J. Park, Appl. Surf. Sci. **181**, 265 (2001).
[9] F. Favot, A. Dal Corso, and A. Baldereschi, Phys. Rev. B **63**, 115416 (2001).
[10] S. G. Wang, D. B. Cao, Y. W. Li, J. G. Wang, and H. J. Jiao, J. Phys. Chem. B **109**, 18956 (2005).
[11] J. Wambach, G. Illing, and H.-J. Freund, Chem. Phys. Lett. **184**, 239 (1991).
[12] R. O. Jones and O. Gunnarson, Rev. Mod. Phys. **61**, 689 (1989).
[13] http://www.pwscf.org and http://www.quantum-espresso.org
[14] J. P. Perdew, K. Burke, and M. Ernzerhof, Phys. Rev. Lett. **77**, 3865 (1996).
[15] J. P. Perdew and A. Zunger, Phys. Rev. B **23**, 5048 (1981).
[16] Ultrasoft pseudopotentials from the publicly available QUANTUM ESPRESSO table are used: Ni.pbe-nd-rrkjus.UPF, O.pbe-rrkjus.UPF, and C.pbe-rrkjus.UPF, and Ni.pz-nd-rrkjus.UPF, O.pz-rrkjus.UPF, and C.pz-rrkjus.UPF for GGA and LDA respectively.
[17] N. Marzari, D. Vanderbilt, and M. C. Payne, Phys. Rev. Lett. **79**, 1337 (1997); M. Methfessel and A. T. Paxton, Phys. Rev. B **40**,

3616 (1989).
[18] *Physics of Solid Surfaces*, edited by G. Chiarotti, Landolt-Börnstein, New Series, Group III Vol. 24, Part C (Springer-Verlag, Berlin 1995).
[19] G. Herzberg, *Electronic Spectra and Electronic Structure of Polyatomic Molecules* (Van Nostrand, New York, 1966).
[20] L. Bengtsson, Phys. Rev. B **59**, 12301 (1999).
[21] B. Meyer and D. Vanderbilt, Phys. Rev. B **63**, 205426 (2001).
[22] A coverage of 1 ML corresponds to 1 CO_2 molecule per surface Ni atom.
[23] H. Jónsson, G. Mills, and K. W. Jacobsen, in *Classical and Quantum Dynamics in Condensed Phase Simulations*, edited by B. J. Berne, G. Ciccotti, and D. F. Coker (World Scientific, Singapore, 1998).
[24] G. Henkelman, B. P. Uberuaga, and H. Jónsson, J. Chem. Phys. **113**, 9901 (2000); **113**, 9978 (2000).
[25] A. Szabo and N. Ostlund, *Modern Quantum Chemistry* (Dover, New York, 1996), p. 153; P. O. Löwdin, J. Chem. Phys. **18**, 365 (1950).
[26] H. Lindner, D. Rupprecht, L. Hammer, and K. Müller, J. Electron Spectrosc. Relat. Phenom. **44**, 141 (1987).
[27] J. Bauhofer, M. Hock, and J. Kippers, Surf. Sci. **191**, 395 (1987).
[28] K. O. Hartman and I. C. Hisatsune, J. Chem. Phys. **44**, 1913 (1966).
[29] B. J. Bandy, M. A. Chesters, P. Hollins, J. Pritchard, and N. Sheppard, J. Mol. Struct. **80**, 203 (1982).
[30] Xunlei Ding, V. Pagan, M. Peressi, and F. Ancilotto, Mater. Sci. Eng., C **27**, 1355 (2007).
[31] D. Alfé, S. de Gironcoli, and S. Baroni, Surf. Sci. **410**, 151 (1998).
[32] K. Wandelt, in *Thin Metal Films and Gas Chemisorption*, edited by P. Wissmann (Elsevier, Amsterdam, 1987).
[33] S. Baroni, S. de Gironcoli, A. Dal Corso, and P. Giannozzi, Rev. Mod. Phys. **73**, 515 (2001).
[34] G. Herzberg, *Infrared and Raman Spectra* (Van Nostrand, New York, 1945).
[35] J. M. Ricart, M. P. Habas, A. Clotet, D. Curulla, and F. Illas, Surf. Sci. **460**, 170 (2000).
[36] X. Wu, M. C. Wargas, S. Nayak, V. Lotrich, and G. Scoles, J. Chem. Phys. **115**, 8748 (2001); D. I. Sayago, J. T. Hoeft, M. Polcik, M. Kittel, R. L. Toomes, J. Robinson, D. P. Woodruff, M. Pascal, C. L. A. Lamont, and G. Nisbet, Phys. Rev. Lett. **90**, 116104 (2003); O. A. von Lilienfeld, I. Tavernelli, U. Rothlisberger, and D. Sebastiani, *ibid.* **93**, 153004 (2004).
[37] H. Rydberg, B. I. Lundqvist, D. C. Langreth, and M. Dion, Phys. Rev. B **62**, 6997 (2000).
[38] M. Dion, H. Rydberg, E. Schröder, D. C. Langreth, and B. I. Lundqvist, Phys. Rev. Lett. **92**, 246401 (2004).
[39] J. B. Neaton, Mark S. Hybertsen, and Steven G. Louie, Phys. Rev. Lett. **97**, 216405 (2006).
[40] A. Kokalj, Comput. Mater. Sci. **28**, 155 (2003); code available from http://www.xcrysden.org/